

AAuAl (A = Ca, Sc, and Ti): Peierls Distortion, Atomic Coloring, and Structural Competition

Joyce Pham[†] and Gordon J. Miller^{*,†,§}

[†]Department of Chemistry, Iowa State University, and [§]U.S. Department of Energy, Ames Laboratory, Ames, Iowa 50011–3111, United States

Supporting Information Placeholder

ABSTRACT: Using density functional theory, the crystal structure variation of AAuAl (A = Ca, Sc, and Ti) from orthorhombic Co₂Si-type to distorted hexagonal Fe₂P-type and then Ni₂In-type structures is shown to correlate with their electronic structures and valence electron counts, sizes of the active metals A, and site preferences for Au and Al atoms, which are arranged to maximize Au–Al nearest neighbor contacts. An evaluation of chemical pressure imposed by the varying A metals using total energy vs. volume calculations indicates that larger unit cell volumes favor the orthorhombic structure whereas smaller volumes favor the hexagonal structures. The electronic origin of the Mg₂Ga-type crystal structure of ScAuAl, refined as a distorted Fe₂P-type supercell doubled along the *c*-axis, indicates a Peierls-type distortion mechanism of the Au-chains along the *c*-axis.

INTRODUCTION

Polar intermetallic compounds containing Au exhibit diverse structures ranging from large clusters and networks of complex polyhedra and even quasicrystals,¹ to smaller atomic coordination spheres and 2-dimensional building blocks.² A defining characteristic of this class is the occurrence of polar-covalent interactions between the formally electropositive metals from groups 1–4 including rare-earth elements, and the more electronegative elements from the late transition metals and early *p*-block. The more electronegative metals form complex clusters or networks with large voids that are filled by the electropositive metals for structural cohesion.³ To date, there lacks a holistic set of fundamental algorithms to predict and rationalize the diverse structures observed for polar intermetallic compounds, such as those like the octet rule, valence electron-to-atom (*e/a*) values, or metallic radius ratios proposed for Zintl-Klemm or Hume-Rothery phases.⁴

A widely used “rule of thumb” to categorize polar intermetallic structures involves using valence electron concentrations (VECs), which are evaluated as the sum of the total number of valence (*s+p+d*) electrons per formula unit (*e/fu*). For the simplest ternary stoichiometry 1:1:1, there are already more than 2000 polar intermetallic compounds reported with many containing Au because it is the most electronegative metal according to Mulliken and Pauling electronegative values.⁵ Some of the commonly observed structures and their corresponding VEC values for 1:1:1 compounds are as follows:^{5–6} (1) orthorhombic TiNiSi (Co₂Si-derivative)-type with 15–18 *e/fu*, and is considered one of the most ubiquitous structure types discussed herein; (2) hexagonal Fe₂P-type with 15–19 *e/fu* but observed mostly for compositions with 18 *e/fu*; and (3) hexagonal CaIn₂- and Ni₂In-type structures, which are observed for compounds with 13–18 *e/fu*. For the 1:1:1 compositions containing Au in the Inorganic Chemistry Structural Database (ICSD), there are 15 compounds in the Fe₂P-type structure, and all except for LuAuAl (17 *e/fu*) and MgAuGa (16 *e/fu*) are reported with In. If Al replaces In in these compounds, the TiNiSi-

type structure is observed instead, and of these 21 compounds with Au, 15 contain both Au and Al, in which all except for CaAuAl (16 *e/fu*) contains 17 *e/fu*. In total, there are 62 compounds containing Au in the CaIn₂- or Ni₂In-type structure, in which only TiAuAl (Ni₂In-type; 18 *e/fu*) contains both Au and Al so that 50 of the 62 compounds all contain 18 *e/fu*. From these VEC trends, it seems that most 1:1:1 polar intermetallic compounds containing both Au and In would crystallize in the Fe₂P-type structure, but that those with both Au and Al would more likely crystallize in the TiNiSi-type, although the Ni₂In-type is plausible as well. However, VEC does not solely distinguish any of these common structure types (Co₂Si/TiNiSi, Fe₂P, and Ni₂In or CaIn₂), so that other factors contributing to the structural variation may be size effects, an understanding of which may be fruitful for investigations using variable pressure to induce structural transitions.

In addition to relationships between VECs and the structure-types discussed above, variations of atomic coordinates in the structure types due to distortions or atomic arrangements (“coloring”)⁷ on going from binary to ternary phases lead to additional structural derivatives. For instance, the Mg₂Ga-type (*hP18*) structure is a subtly distorted supercell of the Fe₂P-type with a doubled *c*-axis, so that ZrNiAl and HfRhSn are ternary derivatives of Fe₂P and Mg₂Ga, respectively.⁸ The question remains about the factors influencing the occurrence of Mg₂Ga-type over its more popular Fe₂P-type subcell. Similarly, within the CaIn₂ family, the isopointal NdPtSb and LiGaGe structures differ in their interlayer interactions along the *c*-axis so that even though both possess hexagonal chair conformations ([Pt₃Sb₃] and [Ga₃Ge₃], respectively) within the puckered honeycomb net of electronegative metal/metalloid atoms, the former exhibits 2-dimensional characteristics whereas the latter features a 3-dimensional tetrahedral network. Again, what factors give rise to these two isopoints within the CaIn₂ structure type?

To contribute to an understanding of the diverse structures among such 1:1:1 polar intermetallics, herein we examine the ScAuAl structure (distorted Fe₂P-type; 17 *e/fu*), which was re-

cently reported to adopt the HfRhSn structure-type (Mg₂Ga ternary derivative).⁹ We discuss its bonding features, electronic structure and stability, atomic size effects and site preferences, and compare its energetics with competing structure types to rationalize the existence of ScAuAl in the Fe₂P-type and its distortion to the Mg₂Ga supercell as opposed to the TiNiSi-, Ni₂In-, and Ca₂In-type structures. Moreover, we perform analogous studies on its neighbors TiNiSi-type CaAuAl (16 *e*⁻/*f**u*) and Ni₂In-type TiAuAl (18 *e*⁻/*f**u*).

EXPERIMENTAL SECTION

Synthesis. ScAuAl was initially found as a product in the search for quasicrystals and their crystalline approximants within the Sc-Au-Al system. A stoichiometric loading confirms its formation using an annealing heating scheme in contrast to the report⁹ of its existence from an arc melting synthesis.

Sc chunks (99.9%, APL-Aldrich), Au spheres (99.99%, Ames Laboratory), and Al ingots (99.999% Alfa-Aesar) were weighed for molar ratios 1Sc: 2Au: 5Al and 1Sc: 1Au: 1Al, with sample sizes totaling 300.0(1) mg. Reaction mixtures were loaded into tantalum ampoules in a glovebox under argon atmosphere, with moisture levels at ≤ 0.1 ppm. The tantalum reaction vessels were then arc-welded shut and subsequently sealed under vacuum in a secondary silica jacket to avoid oxidation of the tantalum during heating to reaction temperatures. All reactions were heated in a tube furnace to 1050 °C for 30 hours, slowly cooled at 10 °C/h to 700 °C and held at this temperature for 15 days, after which they were quenched by rapid submersion into room temperature water.

Powder X-ray Diffraction. Phase analysis was carried out using powder X-ray diffraction (PXRD) data collected on the Stoe Stadi P diffractometer equipped with a position-sensitive image-plate detector and a Cu *K*_{α1} radiation source ($\lambda = 1.54060$ Å). Ground samples were dispersed onto and sandwiched between two transparent acetate films with the aid of vacuum grease. To ensure instrument alignment, a Si powder standard (to compare against sample ICSD # 53783) was mixed with each preliminary scan of the specimen.¹⁰ Data were acquired over a 1-hr exposure period with step sizes of 0.03° in 2 θ , and were analyzed by juxtaposing the observed PXRD patterns against theoretical PXRD patterns calculated from single-crystal XRD refined models and those of reported binary compounds containing the constituent elements.

Single-Crystal XRD. Diffraction data for selected crystals were collected on a Bruker SMART¹¹ APEX II CCD diffractometer with graphite-monochromatized Mo *K*_{α1} radiation ($\lambda = 0.71073$ Å) at ambient conditions between one hemisphere to a full sphere in reciprocal space in ω at 20–30 seconds exposure time per frame.

For the sample chosen from the 1:2:5 loading included in the main text, 2160 frames were collected over an 18 h exposure period and these frames were integrated using the Bruker SAINT software package, which yielded 7792 total peaks in the hexagonal unit cell for θ_{\max} of 31.27° (0.68 Å resolution). The final unit cell parameters were based upon refinements of XYZ-centroids of the 2268 reflections with intensities exceeding 20 σ (I) and scattering angles 2 θ between 11.26° and 62.05°. Data were corrected empirically for absorption using the multi-scan method in the program SADABS,¹² from which the ratio of maximum transparent transmission was 0.446.¹³ Analogously, for the sample chosen from the 1:1:1 loading in the main text, 1800 frames were collected with a total exposure time of 15 h that yielded 4550 total peaks in the hexagonal unit cell for θ_{\max} of 28.87° (0.74 Å resolution). The unit cell parameters were calculated from refinements of XYZ-centroids of the 1329 reflections in scattering angles 2 θ between 11.25° and 56.62° with a ratio of 0.438 maximum transmission. See Tables S1–S4 for additional data sets.

Using the program XPREP,¹⁴ determination of the space group $P\bar{6}2m$ emerged for ScAuAl crystals selected for samples loaded as 1Sc: 2Au: 5Al, so that doubling the *c*-axis to achieve the space group $P\bar{6}2c$ was performed manually. Using the same software, the space group $P62c$ was selected for crystals from sample loadings 1Sc: 1Au: 1Al. All structural models were solved in the SHELXTL 6.14 program suite¹⁵ using direct methods and refined from the full-matrix least-squares fitting of observed structure factors with final refinements that included anisotropic displacements and secondary extinction parameters. The absolute structural parameters were refined to account for the non-centrosymmetric characteristics of $P\bar{6}2m$ and $P\bar{6}2c$.¹⁶ Structure Tidy of the WinGX-Platon program suite was used to standardize the crystallographic sites and to invert and realign the origin of the raw/observed *hkl* data.

Atomic Site Preference, Bader Charge Analysis, Formation Energy, and Electronic Structure. To rationalize the ScAuAl atomic arrangement (“coloring”), first principles electronic structure calculations using VASP 5.2 was carried out on its subcell (Fe₂P-type).¹⁷ The projected augmented wave GGA-PBE method (generalized gradient approximation with exchange correlation potentials as constructed by Perdew, Burke, and Ernzerhof)¹⁸ was employed for six different isocompositional coloring models and their total energies were calculated and compared. For all calculations, the energy cutoff was 500 eV, the self-consistent convergence criterion was 0.01 meV, and the orbital basis set included Sc($3p^6 4s^2 3d^1$), Au($5d^{10} 6s^1$), and Al($3s^2 3p^1$). For each model, the numbers of various interatomic interactions (i.e., Sc-Au/Al, Sc-Sc, and Al/Au-Al/Au,) were assessed to rationalize the atomic site preference of the experimental ScAuAl subcell. Analogous site-preference studies were also performed on the CaAuAl and TiAuAl neighbors with additional orbital bases Ca($3s^2 3p^6 4s^2$) and Ti($3p^6 4s^2 3d^1$).¹⁹ For these site-preference calculations, the reported total energies are from relaxation of the atoms only, so the cell shape and volume were held fixed. To further assess the ordering of Au and Al atoms in ScAuAl, a Bader charge analysis from the results of VASP structural optimizations was carried out on the experimental model of ScAuAl and on “ScCd₂,” in which the atomic sites with the greatest charge were assigned to the more electro-negative metal Au.²⁰ The “ScCd₂” model was examined to provide a uniform frame-of-reference for the Au and Al atoms and so that the total electron count per formula unit is consistent with the experimental ScAuAl if the *d* electrons are considered core.

The AAuAl (A = Ca, Sc, Ti) formation energies ($\Delta E_{\text{reaction}}$) were calculated from the respective elements and reported binary structures Au₂Al, AuAl₂, AAu₂, Au₂A (A = Sc only), AAl₂, and A₂Al (A = Sc only) after VASP optimization, which relaxes the atoms as well as the cell shape and volume.²¹ Additionally, structural optimizations and total energy calculations were carried out for the competing structures: TiNiSi (Co₂Si-derived); NdPtSb, LiGaGe and ScAuSi (all CaIn₂-derived); Ni₂In; and Cu₂Sb.²² For all models, the numbers of interatomic interactions (A-Au/Al, A-A, and Al/Au-Al/Au) per formula unit were evaluated to rationalize the observed AAuAl (A = Ca, Sc, Ti) structural trend. Additionally, chemical pressure effects were investigated using calculated total energies as a function of unit cell volume (*E*(*V*)) for the competing structures CaAuAl (*R*_{Ca} = 1.97 Å; TiNiSi-type), ScAuAl (*R*_{Sc} = 1.64 Å; Fe₂P substructure), and TiAuAl (*R*_{Ti} = 1.47 Å; Ni₂In-type). For these *E*(*V*) calculations, the total energies were from relaxation of only the atoms at fixed volumes. Data were fitted using the Murnaghan potential to extract the volumes with lowest energies and their associated bulk moduli.

The electronic band structures, densities of states (DOS), and crystal orbital Hamilton population (COHP)²³ curves for pair-wise interactions less than 3.4 Å apart were calculated for AAuAl and their various competing structure types using the Stuttgart Tight-Binding Linear Muffin-Tin Orbital Atomic Sphere Approximation (TB-LMTO-ASA) code, with scalar relativistic effects and the von Barth-Hedin local exchange-correlation potential,²⁴ but without

spin-polarization or spin-orbit coupling. Input structural parameters for the TB-LMTO-ASA calculations of ScAuAl used the VASP optimized model of the experimental subcell (Fe₂P-type), whereas those of CaAuAl, TiAuAl, and the other competing structural models were taken from the experimentally reported structures directly.¹⁹ The self-consistent calculation convergence limit was 0.01 meV, the maximum overlap before empty spheres were introduced was 18.7%, and the atomic orbital basis sets contained: Ca(4s, 3d) and Ca(4p, 4f) downfolded; Sc(4s,3d) and Sc(4p) downfolded; Ti(4s, 4p, 3d); Au(6s,6p,5d), and Au(5f) downfolded, Al(3s,3p) and Al(3d) downfolded. The irreducible wedges of the first Brillouin zones used for plotting the DOS and subsequent COHP curves contained 3001 or 5001 *k*-points. See Table S13 for respective atomic Wigner-Seitz radii of each model.²⁵ All graphs and calculations are reported per formula unit, unless designated as per atom.

RESULTS AND DISCUSSION

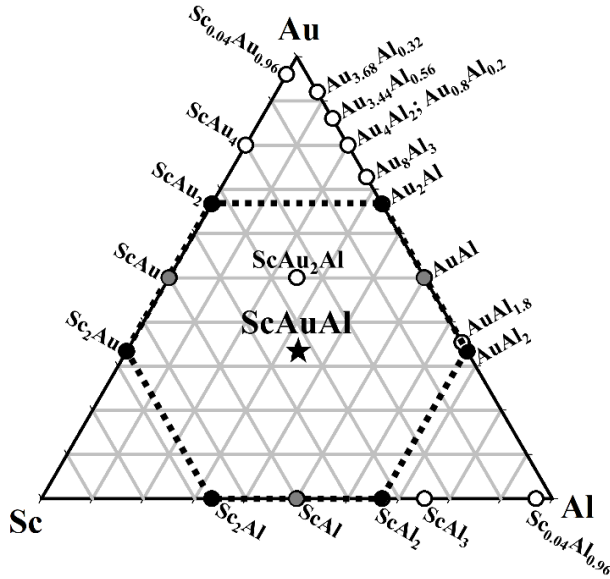


Figure 1. ScAuAl existence triangle showing ScAuAl sitting at the center of the MoSi₂-type ScAu₂, cubic MgCu₂-type ScAl₂, Ni₂In-type Sc₂Al, MoSi₂-type Au₂Al, Co₂Si-type Sc₂Au and CaF₂-type AuAl₂ hexagon (black), with edges bisected by CsCl-type ScAu and ScAl, and monoclinic AuAl (gray).

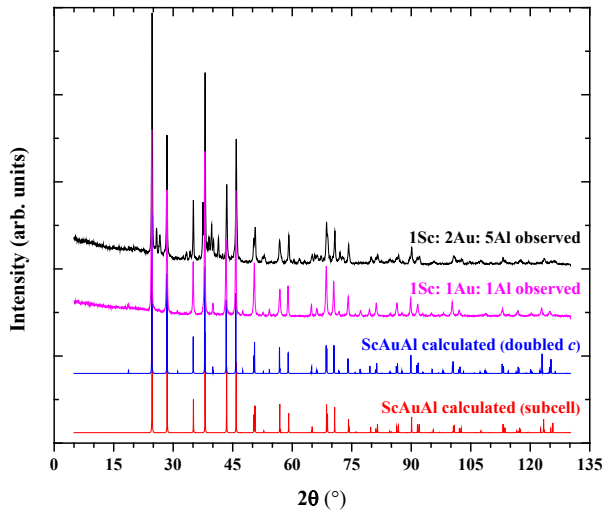


Figure 2. Observed and simulated PXRD patterns from refined single-crystal XRD data for both supercell (Mg₂Ga-type) and subcell (Fe₂P-type) in Sc-Au-Al.

During the search for polar intermetallic quasicrystals and their crystalline approximants in the Ca-Au-Al system^{1b} and as part of a broader investigation on the effects of atomic sizes (chemical pressure) and valence electron counts in such compounds, the Sc-poor region of the Sc-Au-Al system was examined. The loaded molar ratio 1Sc: 2Au: 5Al led to ScAuAl as the major phase with probable traces of at most two of Sc₂Al, ScAl, and ScAl₂ (unequivocal determination of the precise trace phase(s) cannot be made by X-ray powder diffraction). (See Figure S1 for PXRD pattern of the 1Sc: 2Au: 5Al loading with probable binary traces.) ScAuAl sits at the center of the Sc-Au-Al existence triangle (Figure 1), as well as a hexagon formed by tetragonal MoSi₂-type ScAu₂^{21a} and Au₂Al;²⁶ cubic MgCu₂-type ScAl₂^{21b} and CaF₂-type AuAl₂;²⁷ hexagonal Ni₂In-type Sc₂Al;²⁸ and orthorhombic Co₂Si-type Sc₂Au.²⁹ The only other Sc-Au-Al compound reported in the ICSD is the Heusler (AlCu₂Mn)-type ScAu₂Al, which bisects the CsCl-type ScAu and AuAl along the 50% Au-content line.³⁰ In the PXRD pattern from products of the 1Sc: 2Au: 5Al synthesis, the minor phases were assigned as follows: the two peaks at 2θ values ~26–27° were identified as belonging to Sc₂Al²⁸ and ScAl,³¹ and those around 39° and 41° can be indexed for Sc₂Al and ScAl₂^{21b} respectively. However, no single binary or ternary compound from the Sc-Au-Al system could be conclusively assigned to all peaks, a result which calls for analysis using single-crystal XRD for possible new phase(s).

Three crystals were randomly selected from the product of the 1Sc: 2Au: 5Al loading and all crystallographic solutions refined initially to the composition ScAuAl, so that subsequent synthesis of this refined composition and single-crystal XRD analysis of randomly selected specimens from the sample confirmed its formation. However, preliminary structural solutions of crystals selected from the 1Sc: 1Au: 1Al loading differ from the 1Sc: 2Au: 5Al synthesis by a doubling of the unit cell along the *c*-axis in the pure phase sample (see Figure 2 for PXRD patterns). In the PXRD pattern of the doubled *c*-axis structure, the less intense peaks at 2θ values ~19°, 31°, 40°, 48°, 54°, 66°, 72°, and 77° are not clearly visible in the corresponding pattern for the product of the 1Sc: 2Au: 5Al loading. Therefore, subsequent investigations were aimed at assessing the origin of this structural variation by crystallographic refinements and electronic structural studies.

Crystallographic Refinement and Structure. During preliminary stages of this investigation, the structure of ScAuAl was reported to crystallize in the HfRhSn-type structure, which is a derivative of the Mg₂Ga-type and is a slightly distorted superstructure of the Fe₂P-type with a doubled *c*-axis caused by alternating long-short Au-Au chains along the *c*-direction.^{8b, 9} ScAuAl specimens from the sample loaded as 1Sc: 2Au: 5Al yielded structures that can be refined in the Fe₂P-type with acceptable statistical assessment values ($R = 0.016$ for $F^2 > 2s(F^2)$; $wR(F^2) = 0.040$; $R_{int} = 0.032$; and $GOF = 1.21$; see Table S1). For this solution, there are four sites in the asymmetric unit: Au1(1*a*), Au2(2*d*), Al(3*f*, $x = 0.2642(5)$), and Sc(3*g*, $x = 0.5979(3)$), in which Au2(2*d*) and Al(3*f*) lie in the same plane, the 2*d*-2*d* Au₂-Au₂ distances along the *c*-axis are 3.6217(3) Å, and the 2*d*-3*f* Au₂-Al distances in the *ab*-plane are 2.687(4) Å, but the U_{eq} value for the Au2(2*d*) sites is substantially larger by factors of 1.9–2.3 over those for the Au1(1*a*) and Al(3*f*) sites. Manually doubling the unit cell, revising the space group to $P\bar{6}2c$, and assigning the Au₂ sites to two 4*f* sites, each partially occupied but constrained to a total of 4 atoms, led to a refinement with the corresponding *z*-coordinates of the Au₂(4*f*) sites shifted 0.141(7) Å and 0.155(7) Å in opposite directions out of

Table 1. ScAuAl Selected Crystallographic Refinement Parameters

refined composition	ScAu _{1.017(3)} Al _{0.983}				ScAuAl			
instrument					Bruker CCD APEX II			
radiation; λ (Å)/ temp.(K)					Mo K α ; 0.71073/298			
space group/ Pearson					$P\bar{6}2c/hP18$			
loading	1Sc: 2Au: 5Al				1Sc: 1Au: 1Al			
θ range collection/ param.	3.3°–31.3°/ 23				3.3°–29.0°/ 19			
absorp. μ (mm ⁻¹)/ correction	71.83/ empirical				69.90/ empirical			
meas./ indpnt./ obs. [$I > 2\sigma(I)$]/	7249/ 383/ 229				4550/ 307/ 291			
$R[F^2 > 2\sigma(F^2)]/ wR(F^2)/ R_{int}/ GOF$	0.015/ 0.039/ 0.035/ 1.05				0.018/ 0.036/ 0.035/ 1.15			
$\Delta\rho_{max}, \Delta\rho_{min}$ (e Å ⁻³)	1.13, -0.96				1.35, -1.33			
dimensions (Å)	$a = 7.2074(6); c = 7.2443(6)$				$a = 7.2362(10); c = 7.2448(10)$			
volume (Å ³)/ Z	325.90(6)/ 6				328.53(10)/ 6			
index ranges	$-10 \leq h, k \leq 10; -5 \leq l \leq 5$				$-9 \leq h, k, l \leq 9$			
absolute structure param.	0.00(3)				0.03(3)			
$2b, x, y, z, U_{iso}$	Au1		0, 0, 1/4	0.0092(2)	Au1		0, 0, 1/4	0.0077(2)
$4f, x, y, z, U_{iso}$	Au2 (0.54(2))	1/3, 2/3, 0.0195(9)		0.0100(5)	Au2	1/3, 2/3, 0.02100(6)		0.0079(2)
	Au3 (0.42(2))	2/3, 1/3, 0.0214(9)		0.0100(5)	--	--		--
$6g, x, y, z, U_{iso}$	Al/0.016(3)Au	0.2645(5), 0, 0		0.012(1)	Al	0.2628(6), 0, 0		0.0080(7)
$6h, x, y, z, U_{iso}$	Sc	0.4019(7), 0.4024(7), 1/4		0.0137(4)	Sc	0.4096(4), 0.3947(4), 1/4		0.0075(5)
$2b-2b$ (c -axis), $2b-6g, 2b-6h$	3.6221(3)	2.629(1)		2.899(6)	3.6224(5)	2.626(2)		2.912(3)
$4f-4f$ (c -axis), $4f-6g, 4f-6h$	3.312(9),	2.689(2)		2.753(5),	3.3181(8),	2.708(2)		2.831(2),
	3.905(9)			2.942(6)	3.9267(8)			2.887(2)

the Au–Al planes along c and resulting in Au–Au distances of 3.312(9) and 3.905(9) Å. Moreover, the occupancy factor of the Al(6h) site was refined, resulting in 98.4(3)% Al/1.6% Au, and the U_{eq} of all sites were mutually similar in magnitudes. A statistical Hamilton test based on the number of parameters and weighted R -refinement values of the two models show that refinement of the subcell can be rejected up to the 25% significance level.³² Thus, this optimal refinement yields ScAu_{1.017(3)}Al_{0.983} in a disordered Mg₂Ga-type structure. On the other hand, three specimens selected from the 1Sc: 1Au: 1Al loading can be refined directly in the Mg₂Ga-type superstructure with the Au2 (4f) and Al (6g) in the same plane, 4f–4f Au2–Au2 distances alternating at 3.3325(8) and 3.9162(8) Å (average: 3.6244(8) Å) along c , and 4f–6g Au2–Al distances of 2.705(2) Å in the ab -plane. See Tables S2 and S4 for a crystallographic refinement summary.

According to the ICSD, ScAuAl is the only polar intermetallic compound with both Au and Al that crystallizes in the Mg₂Ga-type superstructure and LuAuAl is the only other polar intermetallic with Au and Al adopting the Fe₂P-type substructure. All other members of the LnAuAl series (Ln = Y, Ce to Yb) crystallize in the orthorhombic TiNiSi-type instead, which is also the structure reported for CaAuAl, to be discussed later.³³ The metallic radius of Lu ($R_{Lu} = 1.73$ Å) is smaller than that of the other lanthanides (Ln = Y, Ce to Yb), which vary from 1.75–2.04 Å ($R_{Tm} = 1.75$ Å, $R_{Eu} = 2.04$ Å), so that atomic size seems to play an important factor in the structural variation of A^{III}AuAl (A^{III} = trivalent electropositive metal), which favors the formation of the TiNiSi-type structure for larger electropositive metals, the Fe₂P-type for slightly smaller ones, and the Mg₂Ga-type for the smallest trivalent electropositive atom Sc ($R_{Sc} = 1.64$ Å). Therefore, the unit cell volume of the ScAuAl subcell is smaller (162.90(2) Å³) than that of Fe₂P-type LuAuAl (177.36 Å³), a result arising mainly from a shortening of the c -axis, whereas the a - and b -axes lengthen (from 7.1033(4) Å to 7.2067(6) Å). Additionally, all interatomic contacts shorten on going from LuAuAl to ScAuAl, except the Al–Al interactions, which extend from 3.0758(2) Å to 3.2966(3) Å, and form the triangles of the [Al₃(Au1)₂] trigonal bipyramids in their structures.³³ To highlight the interactions between Au and Al atoms, which are more electronegative than Sc, there are also [Al₃(Au2)₂+Al1] “half-

chair conformers” within the ScAuAl Fe₂P-substructure, features which are related to the [Au₃Ge₃] “chair conformers” in 18 e^-/fu ScAuGe (LiGaGe-type).^{22e} (See Figure S1 for atomic coordination spheres.) On the other hand, for 16 e^-/fu CaAuAl, the orthorhombic TiNiSi-type structure occurs, as seen for LnAuAl (Ln = Y, Ce to Yb), whereas 18 e^-/fu TiAuAl adopts the hexagonal Ni₂In-type structure.¹⁹ Therefore, the structural variation from CaAuAl to ScAuAl to TiAuAl follows along TiNiSi-type to Mg₂Ga-type (Fe₂P-superstructure) to Ni₂In-type, which changes directly with decreasing metallic radius in the electropositive element ($R_{Ca} = 1.97$ Å, $R_{Sc} = 1.64$ Å, $R_{Ti} = 1.47$ Å).

Table 2. ScAuAl Bader Charge Partition Analysis in “Electron Count”

	site	ScAuAl	“ScCd ₂ ”	atom
Fe ₂ P	3g	1.65	1.93	Sc
	1a	13.94	12.50	Au1
	2d	13.26	12.76	Au2
	3f	1.86	12.40	Al
Mg ₂ Ga	6h	1.64	1.91	Sc
	2b	13.82	12.44	Au1
	4f	13.30	12.77	Au2
	6g	1.88	12.43	Al

Atomic Site Preference. Since the crystallographic refinements of ScAuAl yield structures that are subtle distortions from the hexagonal Fe₂P-type, the site preferences for different elements were analyzed using the smaller subcell (the calculated total energy of the experimental structure is just 6 meV lower than that of the Fe₂P model). Evaluating atomic colorings of a structural network involves evaluating factors contributing to the site energy and bond energy terms of the total band energy.⁷ The site energy term can be qualitatively assessed using a Bader charge analysis on models that use the same atomic potentials for the sites being examined for differentiation. For ScAuAl, Bader charge analyses of ScAuAl and hypothetical “ScCd₂” in both the Fe₂P- and Mg₂Ga-type structures corroborate the experimental coloring (see Table 2). For all models, the charges on the 1a (2b) and 2d (4f) sites are greater than those on the 3f (6g) sites and indicate their respective preferences for Au and Al based on their relative electronegativities.

Table 3. ScAuAl Atomic Site Preference from Isocompositional Coloring Models.

(Å)	Experiment	α	β	γ	δ	ϵ
< 2.7	Au–Al (12×)	Au–Al (12×)	Sc–Au (12×)	Sc–Au (12×)	Sc–Al (12×)	Sc–Al (12×)
< 2.9	Sc–Au (15×)	Sc–Al (15×)	Au–Al (15×)	Sc–Al (15×)	Au–Al (15×)	Sc–Au (15×)
< 3.2	Sc–Al (18×)	Sc–Au (18×)	Sc–Al (16×)	Au–Al (16×)	Sc–Au (18×)	Au–Al (18×)
< 3.4	Al–Al (3×)	Au–Au (3×)	Sc–Sc (3×)	Au–Au (3×)	Sc–Sc (3×)	Al–Al (3×)
eV/f.u.	0	+0.347	+0.960	+1.480	+1.759	+2.112

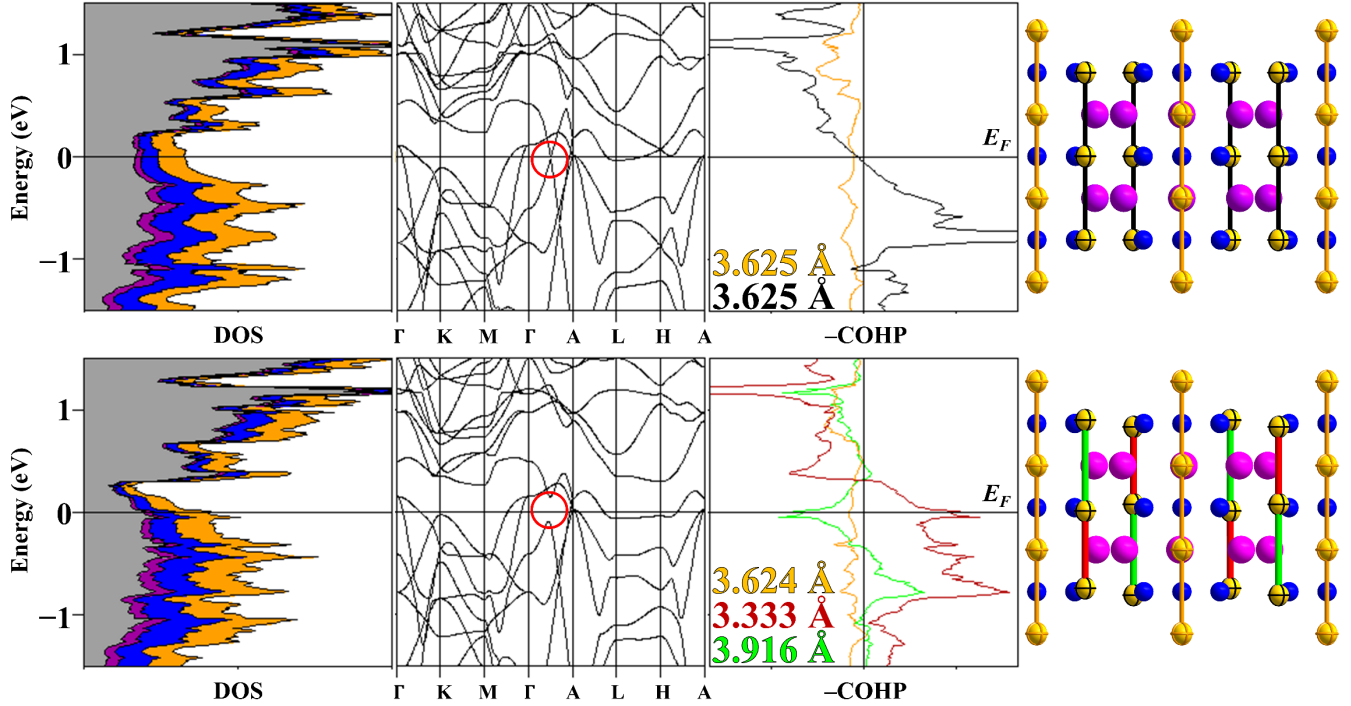


Figure 3. ScAuAl electronic structures in the Fe_2P -type subcell (top) and Mg_2Ga -type supercell (bottom) with Au–Au pseudo Peierl’s distortion. For all COHP curves, (–) and (+) respectively indicate antibonding and bonding. Sc is in dark purple, Au is in dark yellow and Al is blue. Sc(3*d*) orbital contribution in the DOS is in gray.

To examine the bond energy term in ScAuAl, interatomic distances less than 3.4 Å, which is 0.14 Å greater than the Sc–Sc distances in hcp Sc, were taken into account in the Fe_2P -type model. Thus, there are seven different interatomic contacts (2.638(5), 2.681(1), 2.848(5), 2.893(5), 3.005(6), 3.125(3), and 3.331(2) Å) to account for in ScAuAl, and, for space group $P\bar{6}2m$ (no. 189), there are six different atomic arrangements that can be generated by switching elements among the various crystallographic sites to maintain the overall composition ScAuAl. According to the results of VASP total energy calculations for each coloring, listed in Table 2 (and Table S5), the lowest energy occurs for the experimental model, which maximizes the number of shortest Au–Al interactions, followed by the next shortest distances of Sc–Au interactions so that Sc–Al and Al–Al distances are respectively longer. The next most energetically competitive model in this set (coloring α in Table 2) also has shortest Au–Al interactions, but the next shortest distances are Sc–Al contacts rather than Sc–Au. Therefore, ScAuAl prefers shorter Sc–Au over Sc–Al contacts, which can be influenced by the greater polar character of Sc–Au over Sc–Al interactions, as well as stabilizing Sc–Au interactions between nearly empty 3*d* atomic orbitals of Sc with formally filled 5*d* AOs of Au. Model β has overall more total Au–Al interactions (15×) at distances less than 3.4 Å than both the experimental

and α model, but these interactions are not amongst the shortest distances, which suggests that ScAuAl prefers to maximize the number of shortest Au–Al interactions over a greater frequency of Au–Al interactions at longer averaged distances, in general, and that the next shortest distances favor Sc–Au over Sc–Al contacts. This atomic site preference analysis based on interatomic interactions also supports a structure that can be broken up into “planes” of $[(\text{Au}_2)_2\text{Al}_3]$ and $[\text{Sc}_3(\text{Au}1)]$ stacked alternately along the *c*-axis as mentioned in the atomic structure discussion. The preference for shorter Sc–Au contacts is also observed in nonstoichiometric $\text{ScAu}_{1.017(3)}\text{Al}_{0.983}$, which is refined from selected specimens in the 1Sc: 2Au: 5Al molar loading. Here, the sites Au3/Au2 that split along the *c*-axis out of the $[\text{Au}_2\text{Al}_3]$ plane lead to overall more number of Sc–Au shorter distances (2.754(5) Å (3×); (2.946(5) Å (3×)) than in the case without the splitting (Sc–Au: 2.845(3) Å (6×)).

Like ScAuAl, TiNiSi-type CaAuAl also exhibits shortest Au–Al distances followed by Ca–Au, with longer Ca–Al distances.^{19a} In TiAuAl, Au–Al distances are also the shortest, whereas Ti–Ti and Ti–Au/Al are comparable,^{19b} which implies enhanced A–A (Ti–Ti) bonding than in the other AAuAl structures (A = Ca or Sc). In the structures of many ternary polar intermetallic compounds, such as these AAuAl examples with two different electronegative metallic components, maximizing the number

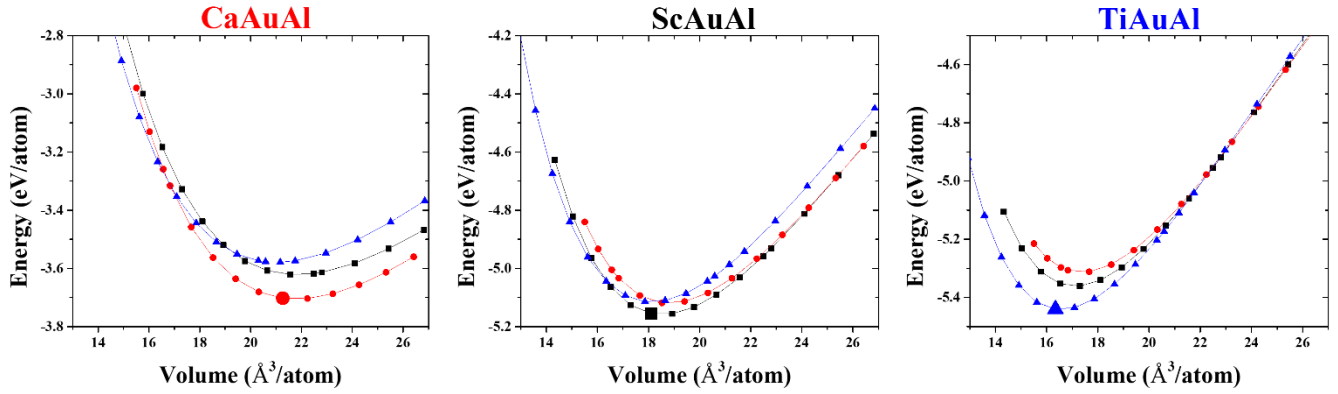


Figure 4. AAuAl total energies as a function of volume in competing models: TiNiSi as observed for CaAuAl in red; Fe₂P refined for ScAuAl in black, and Ni₂In as observed for TiAuAl in blue. For each, the experimental model is shown as a larger data point.

Table 4. AAuAl (A = Ca, Sc, Ti) Formation Energies (eV/f.u.)

Sc + Au + Al \longrightarrow ScAuAl	-2.308
$\frac{1}{2}$ ScAu ₂ + $\frac{1}{2}$ ScAl ₂ \longrightarrow ScAuAl	-0.348
$\frac{1}{2}$ Sc ₂ Al + $\frac{1}{2}$ Au ₂ Al \longrightarrow ScAuAl	-1.313
$\frac{1}{2}$ Sc ₂ Au + $\frac{1}{2}$ AuAl ₂ \longrightarrow ScAuAl	-0.663
Ca + Au + Al \longrightarrow CaAuAl	-2.142
$\frac{1}{2}$ CaAu ₂ + $\frac{1}{2}$ CaAl ₂ \longrightarrow CaAuAl	-0.569
Ti + Au + Al \longrightarrow TiAuAl	-1.522
$\frac{1}{2}$ TiAu ₂ + $\frac{1}{2}$ TiAl ₂ \longrightarrow TiAuAl	-0.226

of shortest distances between the more electronegative elements, i.e., Au and Al, while manifesting a large number of stabilizing polar-covalent A-(Au+Al) interactions subject to the size constraints of A reflects one of the hallmarks of this compound class.^{1b, 4a}

Electronic Origins of the Distortion from Fe₂P-type to Mg₂Ga-type in ScAuAl. As indicated by our crystallographic refinements and a previous investigation,⁹ ScAuAl is slightly distorted from the Fe₂P-type structure. The calculated electronic DOS curve, band structure, and Au–Au COHP curves (see Figure 3) for Fe₂P-type ScAuAl reveal distinct similarities to a Peierls-like distortion, because at the Fermi level the band structure shows a degeneracy via band crossing near the midpoint wavevector between the $\Gamma(0,0,0)$ and $A(0,0,c^*/2)$ and the Au₂–Au₂ COHP curve crosses from bonding states below to antibonding states above the Fermi level. Upon distortion of the structure to create alternating Au–Au distances along the c -axis, the degeneracy is broken in the band structure, the Fermi level falls within the gap for these states at $\mathbf{k} \sim (0, 0, c^*/4)$, and, as seen in the COHP curve (Figure 3), the shorter and longer Au–Au distances give, respectively, occupied bonding and antibonding states at the Fermi level.

The Peierls-like distortion is observed for chains formed by the Au₂ atoms only, and not those by Au₁, a result that leads to shorter Sc–Au distances. Half of the interplanar Sc–Au distances (2.852(3) Å) of the subcell become shorter on going to the distorted structure (2.826(4) and 2.886(3) Å), but remain the same on average. On the other hand, all Au–Al distances remain the same (interplanar: 2.624(5) vs. 2.622(4) Å; intraplanar: 2.699(4) to 2.704(3) Å). Thus, the distortion implies a strong preference for Sc(3d)–Au(5d) interactions, as also seen by the Sc 3d-partial orbital breakdown of the electronic DOS

(Figure 3) and atomic site preferences for Sc–Au near neighbors (Table 3).

Formation Energies. The theoretical energy of formation provides information on the stability of a compound and the feasibility of assembling the structure from its constituent starting reagents. AAuAl (A = Ca, Sc, Ti) formation energies calculated from the elements and their corresponding binaries $\frac{1}{2}$ AAu₂ + $\frac{1}{2}$ AAl₂ show that, in general, the formations of the ternaries are all energetically favorable (Table 4), and that computational studies and experimental structural reports of AAuAl corroborate one another. Additionally, whereas the formation of ScAuAl from the elements is most energetically favorable in comparison to that of (Ca/Ti)AuAl, formation of CaAuAl from CaAu₂ and CaAl₂ is more favorable than formation of (Sc/Ti)AuAl from their binaries. This type of calculation provides some insight into the potential use of binary precursors for the synthesis of a ternary compound.

Competing Structural Models. Differences in AAuAl (A = Ca, Sc, Ti) formation energies are much larger than differences in energies between related structures, so that, in general, the factors giving rise to a compound in a specific structure is an investigation that utilizes and analyzes calculated electronic structures, atomic site preferences, and relative atomic characteristics such as size and electronegativity.

From CaAuAl to ScAuAl to TiAuAl, the overall decreasing unit cell volume ($V_{\text{CaAuAl}} = 21.324 \text{ \AA}^3/\text{atom}$; $V_{\text{ScAuAl}} = 18.103 \text{ \AA}^3/\text{atom}$; and $V_{\text{TiAuAl}} = 16.344 \text{ \AA}^3/\text{atom}$) reflects the decreasing metallic radius of the formally electropositive element ($R_{\text{Ca,Sc,Ti}} = 1.97, 1.64, 1.47 \text{ \AA}$). For the elements themselves, these decreasing metallic radii correspond to filling metal–metal bonding states of the 3d band, so we may anticipate similar features for the electronic structures of these ternary intermetallics. The size effect from the electropositive metal is also demonstrated by LnAuAl (Ln = rare-earth metals)³³ adopting the orthorhombic TiNiSi-type as opposed to hexagonal Mg₂Ga- (doubled, distorted Fe₂P-) type for ScAuAl. To examine this size effect of the A elements, total energy vs. volume, $E(V)$, curves were calculated for AAuAl (A = Ca, Sc, Ti) in the three competing TiNiSi-, Fe₂P-, and Ni₂In-type models (Figure 4), all of which show smaller energy differences among the three structures than the calculated total energies of formation. For each AAuAl, the crystallographically determined structure type gives the lowest overall energy and the corresponding unit cell volume agrees with the experimental value. A comparison of the three sets of $E(V)$ curves indicates that the sizes of the electropositive A metals play a significant role for the structures of these

Table 5. Calculated Murnaghan Minimum Energy E_0 (eV/atom), Volume V_0 ($\text{\AA}^3/\text{atom}$), and Bulk Modulus B_0 (Mbar) and its derivative B_0'

Type	Compound		
	CaAuAl	ScAuAl	TiAuAl
TiNiSi	-3.705; 21.850; 0.6744; 4.156	-5.118; 18.773; 1.0506; 5.059	-5.314; 17.322; 1.3159; 5.946
Fe2P	-3.622; 21.920; 0.6411; 4.026	-5.155; 18.508; 1.0496; 4.956	-5.361; 17.019; 1.3038; 5.740
Ni2In	-3.580; 21.137; 0.6599; 3.920	-5.110; 18.138; 1.0105; 4.649	-5.437; 16.474; 1.2757; 5.361

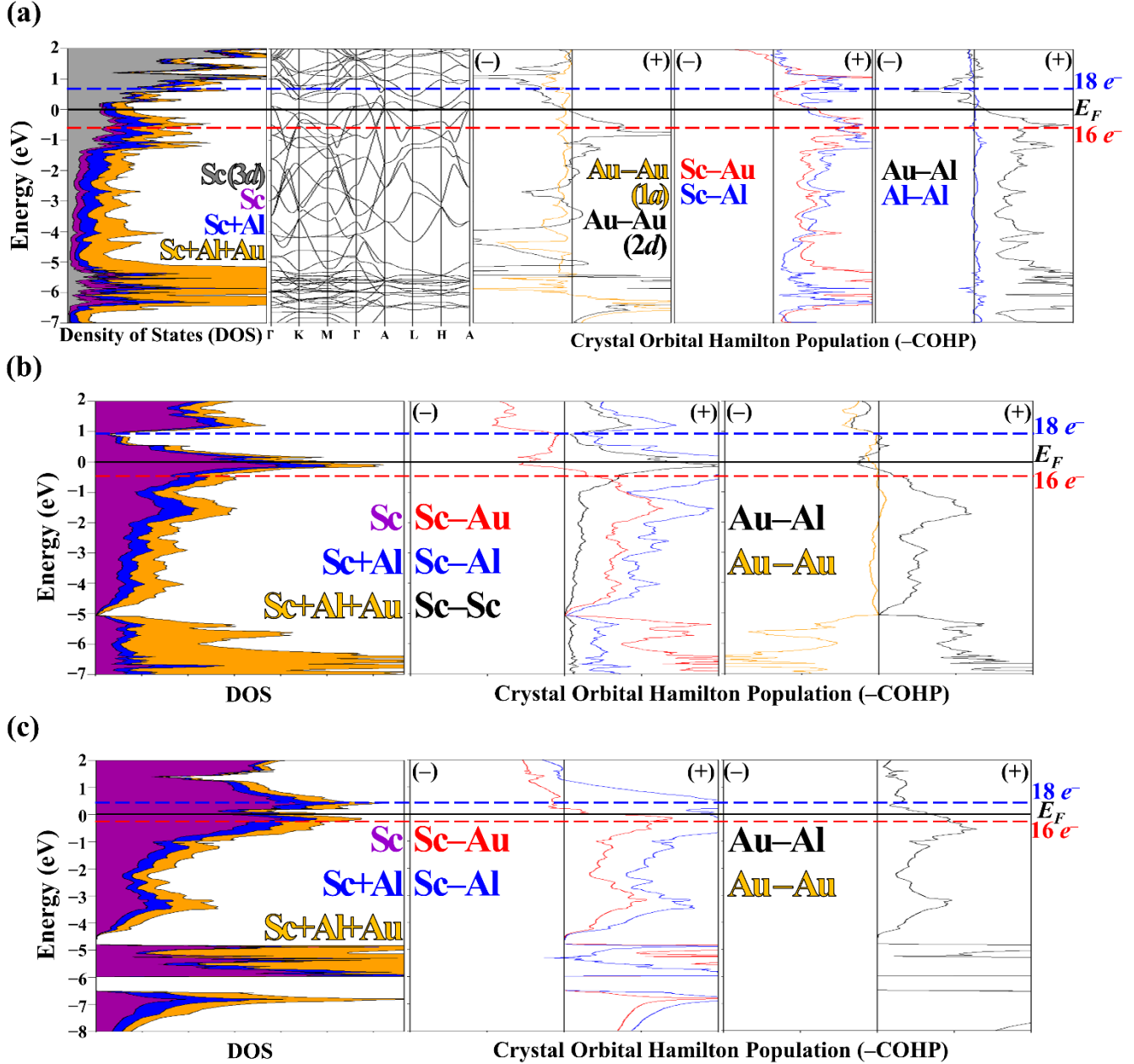


Figure 5. ScAuAl in the (a) experimental, (b) TiNiSi-type and (c) Ni₂In-type as respectively seen for CaAuAl and TiAuAl. For all COHP curves, (-) and (+) indicate antibonding and bonding, respectively for contacts < 3.5 Å.

16–18 e^-/fu AAuAl compounds: (a) at large volumes, the TiNiSi-type structure is favorable (it becomes energetically competitive for ScAuAl at $\sim 10\%$ above V_{exp} and for TiAuAl at $\sim 11\%$ above V_{exp}); and (b) at small volumes, the hexagonal Ni₂In-type structure is favorable (it becomes competitive for ScAuAl at $\sim 3\%$ below V_{exp} and for CaAuAl at $\sim 7\%$ below V_{exp}). These results imply that under pressure, ScAuAl may transform into a

hexagonal Ni₂In-type; CaAuAl is also susceptible to this transformation but the pressure would be much higher than for ScAuAl. Furthermore, fitting all curves using a Murnaghan form (Table 5) shows that the bulk moduli for all TiNiSi-type curves are the largest.

Besides atomic size effects, analysis of interatomic interactions arising from atomic site preferences in the observed and

Table 6. AAuAl Competing Models, Total Energies, and Integrated COHP < 3.5 Å

ScAuAl (Fe₂P-type)							
	TiNiSi	Fe ₂ P	Ni ₂ In	NdPtSb	LiGaGe	ScAuSi	
$\Delta E(eV/f.u.)$	+0.031	0.000	+0.081	+0.077	+0.079	+0.140	
a (Å)	6.674	7.287	4.467	4.459	4.459	4.427	
b (Å)	4.378						
c (Å)	7.636	3.625	6.389	6.419	6.428	6.623	
V (Å ³ /f.u.)	55.779	55.563	55.191	55.257	55.333	56.213	
-ICOHP (%)	Sc-Au	27.95	19.12	30.24	29.23	29.26	37.36
	Sc-Al	23.16	15.33	26.99	26.74	23.83	31.47
	Sc-Sc	4.59	--	--	--	1.54	4.48
	Au-Al	38.73	64.39	42.77	44.03	45.38	22.52
	Al-Al	--	1.16	--	--	--	2.36
	Au-Au	5.57	--	--	--	--	1.80
CaAuAl (TiNiSi-type)							
	TiNiSi	Fe ₂ P	Ni ₂ In	NdPtSb	LiGaGe	ScAuSi	
$\Delta E(eV/f.u.)$	0.000	+0.138	+0.216	+0.213	+0.217	+0.212	
a (Å)	7.337	7.255	4.548	4.563	4.564	4.536	
b (Å)	4.552						
c (Å)	7.824	4.310	7.597	7.526	7.513	7.703	
V (Å ³ /f.u.)	65.319	65.485	68.043	67.836	67.752	68.642	
-ICOHP (%)	Ca-Au	21.83	14.59	28.35	27.09	23.31	34.55
	Ca-Al	19.94	13.36	26.12	25.27	21.60	30.57
	Ca-Ca	--	--	--	--	1.03	2.89
	Au-Al	55.93	70.73	45.53	47.65	52.05	26.97
	Al-Al	2.31	1.32	--	--	--	2.98
	Au-Au	--	--	--	--	--	2.04
TiAuAl (Ni₂In-type)							
	TiNiSi	Fe ₂ P	Ni ₂ In	NdPtSb	LiGaGe	ScAuSi	
$\Delta E(eV/f.u.)$	+0.234	+0.157	0.000	+0.020	+0.024	+0.121	
a (Å)	6.516	6.694	4.461	4.365	4.363	4.395	
b (Å)	4.001						
c (Å)	7.747	3.977	5.740	6.150	6.161	6.025	
V (Å ³ /f.u.)	50.494	51.435	49.452	50.740	50.788	50.392	
-ICOHP (%)	Ti-Au	33.83	24.72	34.01	39.69	35.05	40.21
	Ti-Al	27.78	21.33	27.62	32.19	28.66	34.51
	Ti-Ti	5.43	--	6.65	--	4.25	8.98
	Au-Al	28.50	52.98	31.72	28.12	32.04	13.97
	Al-Al	--	0.97	--	--	--	1.26
	Au-Au	4.46	--	--	--	--	1.06

competing models provide effective rationale for the observed structural variations. These are obtained by calculated electronic DOS and COHP curves for nearest pairwise interactions for distances less than 3.5 Å. Since the observed structures (TiNiSi-type for 16 e^-/fu CaAuAl; distorted Fe₂P-type for 17 e^-/fu ScAuAl; and Ni₂In-type for 18 e^-/fu TiAuAl) all contain [AuAl] networks involving [Au₃Al₃] alternant hexagonal rings, three additional structure types based upon the hexagonal CaIn₂-type were examined: (1) NdPtSb-type, observed for CeAuGe, but contains no Au-Ge interactions along the c -direction yielding essentially separated puckered hexagonal [Au₃Ge₃] layers; (2) LiGaGe-type, which occurs for ScAuGe, and have a 3D tetrahedral framework with only Au-Ge contacts; and (3) ScAuSi features [Au₃Si₃] puckered hexagons stacked directly on top of one another with distances that suggest Au-Au and Si-Si interlayer interactions.²² Geometrically, the hexagonal layers of the electronegative metal/metalloid network in CaIn₂-type derivatives are puckered in a chair-conformation; those in Ni₂In-type (TiAuAl) are planar; and those in the distorted Fe₂P-type (ScAuAl) are half-chair conformers.

Table 6 summarizes the total energies, relative to the lowest energy structure, calculated unit cell parameters, and percent integrated Hamilton populations (ICOHPs) evaluated for all interactions within 3.5 Å for AAuAl (A = Ca, Sc, and Ti) in the various competing models (see Tables S6–S11 for more details). Some general observations of the results in Table 6 include: (i)

for all AAuAl, the total energies for hexagonal Ni₂In- and CaIn₂-derivatives, except for the ScAuSi-type, fall within a few millivolts of each other; (ii) the lowest energy structures for CaAuAl and TiAuAl exhibit the smallest unit cell volumes per formula unit; and (iii) the Fe₂P-structure type always shows the greatest polar-covalent bonding contributions coming from Au–Al contacts for all AAuAl cases.

Examination of the DOS and COHP curves for these cases can illuminate these outcomes. Figure 5 shows these curves for 17 e^-/fu ScAuAl in Fe₂P-, TiNiSi-, and Ni₂In-type arrangements. The different structures significantly affect the shapes of the DOS curves. For the Fe₂P-type, there are no clear gaps in the DOS, although the Au 5d band is clearly seen at 5 eV below the Fermi level and is about 1.5 eV wide. At the Fermi level, there is a pseudogap arising from the general crossing of Sc 3d states with Au 6s and 6p orbitals (the rationale for the distortion of ScAuAl was given earlier). This pseudogap region also corresponds to essentially optimized Au–Al interactions, but there remain Sc–Au and Sc–Al bonding states above E_F as seen in their COHP curves in Figure 5. By applying a rigid-band approximation to these curves, for 16 e^-/fu , significant Au–Al states would be depleted, whereas for 18 e^-/fu , Au–Al antibonding states would be populated. The DOS curves for ScAuAl in the TiNiSi- and Ni₂In-alternatives show distinct (pseudo)gaps for 12 electrons, which correspond to formally filling one s -band and the Au 5d band with electrons. The Fermi levels for 17 e^-/fu both lie close or on peaks in the DOS curve, and the Ni₂In-type DOS shows considerable contributions from Sc wavefunctions among the occupied states. Therefore, the Fe₂P-related structure adopted by ScAuAl optimizes Au–Al interactions while avoiding Sc–Au antibonding interactions, which are indicated for TiNiSi-type “ScAuAl” in its COHP curve. (See Figure S2 for electronic structures of ScAuAl in competing structures related to CaIn₂: NdPtSb- LiGaGe-, and ScAuSi.)

Analogous analyses are afforded for the (Ca/Ti)AuAl neighbors to rationalize features stabilizing their observed structures. In TiNiSi-type CaAuAl, the next most competitive model to the experimental one is the Fe₂P-type structure; in both, Au–Al interactions contribute the most to the total ICOHP value, as in ScAuAl. (See Tables S8–S9 for summaries and Figure S3 for electronic structures of CaAuAl in competing structure types.) Also like ScAuAl, there are overall bonding Ca–Au and Ca–Al interactions at the Fermi level, but unlike ScAuAl the Au–Al interactions are not optimized. The small volume of the unit cell relative to the other structural models reflects that there may be significant stabilization arising from charge transfer from Ca to the electronegative Au and Al atoms in this structure. In Ni₂In-type TiAuAl, the observed Ni₂In- and CaIn₂-type models are energetically close, which is somewhat surprising given that the [Au₃Al₃] hexagons in the CaIn₂-type variants are puckered whereas those in the Ni₂In-type are planar. For the observed structure of TiAuAl, the Au–Al distances are the shortest (2.5448(5) Å), followed by the Ti–Ti distances (2.9145(5) Å) (See Tables S10–S11 for summaries of TiAuAl and its competing structure types and Figure S4 for electronic structures.) According to analysis of the ICOHPs (Table 6), the Ni₂In-type structure yields a nearly even distribution in bonding contributions from Au–Al, Ti–Au, and Ti–Al interactions, while also providing some Ti–Ti bonding. The CaIn₂-types show similar characteristics, but with some subtle redistribution in bonding contributions, results which rationalize the similar total energies to the Ni₂In-type model. On the other hand, the relative destabilization of TiNiSi- and Fe₂P-types occurs, respectively, by introducing either Au–Au interactions or

reducing the contributions of Ti–Au and Ti–Al to the total bond energy term.

CONCLUSIONS

AAuAl (A = Ca, Sc, Ti) compounds with consecutively increasing valence electron concentration (16–18 e^-/fu) and decreasing atomic radius crystallize in different structure types: orthorhombic TiNiSi-type CaAuAl; hexagonal Mg₂Ga-type ScAuAl (a distorted superstructure of Fe₂P-type); and hexagonal Ni₂In-type TiAuAl. Density functional theory and atomic site preference investigations using total energy calculations show that this structural variation is related to both chemical pressure effects, results indicating larger unit cells favoring the orthorhombic TiNiSi structure and smaller unit cells favoring the hexagonal Fe₂P- or Ni₂In-type structure, as well as atomic arrangements that maximize the number of Au–Al nearest neighbor contacts. Electronic DOS and COHP plots highlight the polar covalent A–(Au+Al) interactions, which are also necessary for structural cohesion. For the ScAuAl structure specifically, the electronic band structure and Au–Au COHP curves indicate that the refined Mg₂Ga-type structure arises from a Peierls-like distortion of the Au-chains along the *c*-axis, which gives rise to the doubled *c*-axis on going from the Fe₂P- to Mg₂Ga-type structures.

ASSOCIATED CONTENT

Supporting Information (SI) with the following is available free of charge on the ACS Publications website: Phase analysis of the 1Sc: 2Au: 5Al loading; Environment of each atom in the ScAuAl asymmetric unit of Fe₂P structure; Selected crystallographic parameters of ScAuAl refined in the Fe₂P-structure as selected from the 1Sc: 2Au: 5Al molar loading as well as the Mg₂Ga-structure as selected from the 1Sc: 1Au: 1Al molar loading; ScAuAl (Fe₂P-structure), CaAuAl (TiNiSi-structure), and TiAuAl (Ni₂In-structure) relative total formation energies and energies of competing structures with numbers of selected interatomic distances; ScAuAl structural parameters after VASP optimization used for subsequent electronic calculations; Ca, Sc, Ti, Au, and Al Wigner Seitz radii; DOS and COHP curves of AAuAl in all competing structure types.

AUTHOR INFORMATION

Corresponding author

*E-mail: gmill@iastate.edu

Notes

The authors declare no competing financial interest.

ACKNOWLEDGEMENTS

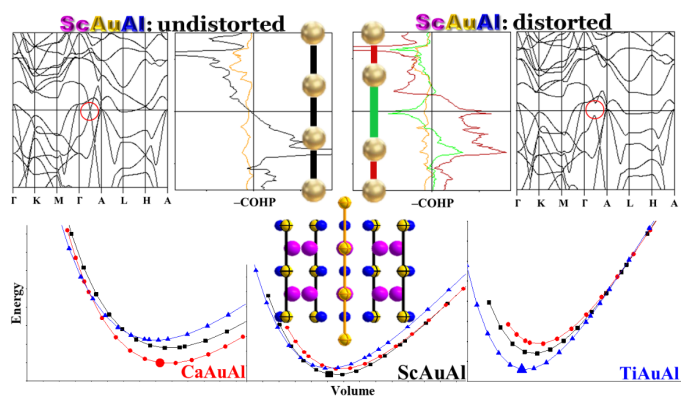
The authors are grateful for funding from the U.S. National Science Foundation (Grant DMR 10-05765). Diffraction instrumentation was provided by support of the Basic Energy Sciences, Materials Sciences Division, U.S. Department of Energy at Ames Laboratory, which is operated by Iowa State University under contract no. DE-AC02-07CH11358. All computational investigations were performed on the CRUNCH system supported by the Iowa State University Computation Advisory Committee Project no. 202-17-10-08-0005.

REFERENCES

- (a) Miller, G. J.; Thimmaiah, S.; Smetana, V.; Palasyuk, A.; Lin, Q. Gold's Structural Versatility Within Complex Intermetallics: From Hume-Rothery to Zintl and Even Quasicrystals *Mater. Res. Soc. Symp. Proc.* **2013**, *1517*; (b) Pham, J.; Kreyssig, A.; Goldman, A. I.; Miller, G. J. An Icosahedral Quasicrystal and Its 1/0 Crystalline Approximant in the Ca–Au–Al System *Inorg. Chem.* **2016**, *55*, 10425–10437.
- Palasyuk, A.; Grin, Y.; Miller, G. J. Turning Gold into “Diamond”: A Family of Hexagonal Diamond-Type Au-Frameworks Interconnected by Triangular Clusters in the Sr–Al–Au System *J. Am. Chem. Soc.* **2014**, *136*, 3108–3117.
- (a) Miller, G. J.; Lee, C.-S.; Choe, W. Structure and Bonding Around the Zintl Border. In *Inorganic Chemistry Highlights*; Meyer, G.; Naumann, D.; Wesemann, L., Eds.; Wiley-VCH: Weinheim, Germany, **2002**; pp 21–53; (b) Miller, G. J.; Schmidt, M.; Wang, F.; You, T.-S. Quantitative Advances in the Zintl–Klemm Formalism *Structure and Bonding* (Zintl Phases) **2011**, *139*, pp 1–55.
- (a) Miller, G. J.; Reedijk, J.; Poeppelmeier, K. R. Metal-Rich Compounds of the *d*-Metals. *Comprehensive Inorganic Chemistry II* **2013**, *2*, 311–357; (b) Nesper, R. Bonding Patterns in Intermetallic Compounds *Angew. Chem. Int. Ed. Engl.* **1991**, *30*, 789–817.
- (a) Dshemuchadse, J.; Steurer, W. More Statistics on Intermetallic Compounds–Ternary Phases *Acta Crystallogr. Sect. A* **2015**, *71*, 335–345; (b) Bojin, M. D.; Hoffmann, R. The RE–M–E Phases-Overview *Helv. Chim. Acta.* **2003**, *86*, 1653–1682.
- (a) Bojin, M. D.; Hoffmann, R. The RE–M–E Phases–What's Possible *Helv. Chim. Acta.* **2003**, *86*, 1683–1708; (b) Seibel, E. M.; Schoop, L. M.; Xie, W.; Gibson, Q. D.; Webb, J. B.; Fuccillo, M. K.; Krizan, J. W.; Cava, R. J. Gold–Gold Bonding: The Key to Stabilizing the 19-Electron Ternary Phases LnAuSb (Ln = La–Nd and Sm) *J. Am. Chem. Soc.* **2015**, *137*, 1282–1289.
- Miller, G. J. The “Coloring Problem” in Solids: How it Affects Structure, Composition and Properties *Eur. J. Inorg. Chem.* **1998**, *1998*, 523–536.
- (a) Zumdick, M. F.; Hoffmann, R.-D.; Pöttgen, R. The Intermetallic Zirconium Compounds ZrNiAl, ZrRhSn, and ZrPtGa – Structural Distortions and Metal-Metal Bonding in Fe₂P Related Compounds *Z. Naturforsch. B.* **1999**, *54b*, 45–53; (b) Zumdick, M. F.; Pöttgen, R. Determination of the Superstructures for the Stannides ZrIrSn, HfCoSn, and HfRhSn *Z. Kristallogr. Cryst. Mater.* **1999**, *214*, 90–97.
- Radzieowski, M.; Benndorf, C.; Haverkamp, S.; Eckert, H.; Janka, O. On New Ternary Equiatomic Scandium Transition Metal Aluminum Compounds ScTAl with T = Cr, Ru, Ag, Re, Pt, and Au *Z. Naturforsch. B.* **2016**, *71*, 553–566.
- Kuestner, H. R. Struktur des Siliziums *Physikalische Zeitschrift* **1923**, *24*, 25–29.
- SMART, version 5; Bruker AXS: Madison, WI, **2003**.
- Sheldrick, G. M. SADABS; University of Gottingen: Gottingen, Germany, **2001**.
- Blessing, R. An Empirical Correction for Absorption Anisotropy. *Acta Crystallogr., Sect. A* **1995**, *51*, 33–38.
- Sheldrick, G., SHELX, version 6.14; Bruker AXS: Madison, WI, **2000–2003**.
- Sheldrick, G., A Short History of SHELX. *Acta Crystallogr. Sect. A* **2008**, *64*, 112–122.
- Parsons, S.; Flack, H. D.; Wagner, T. Use of Intensity Quotients and Differences in Absolute Structure Refinement. *Acta Crystallogr. Sect. B* **2013**, *69*, 249–259.

17. (a) Blöchl, P. E. *Phys. Rev. B* **1994**, *50*, 17953; (b) Kresse, G.; Hafner, J. *Phys. Rev. B* **1993**, *47*, 558; (c) Kresse, G.; Furthmüller, F. *Comput. Mater. Sci.* **1996**, *6*, 15.
18. Perdew, J. P.; Burke, K.; Ernzerhof, M. Generalized Gradient Approximation Made Simple *Phys. Rev. Lett.* **1996**, *77*, 3865.
19. (a) Cordier, G.; Friedrich, T. Crystal Structure of Calcium Gold Aluminium (1/1/1), CaAuAl *Z. Kristallogr. Cryst. Mater.* **1992**, *201*, 304–305; (b) Jorda, J. L.; Muller, J.; Braun, H. F.; Susz, C. Phase Relationships in the Ternary System Ti–Au–Al at 775 K. *J. Less Common Met.* **1987**, *134*, 99–107.
20. Bader, R. F. W. *Atoms in Molecules: A Quantum Theory*. Clarendon Press: **1994**.
21. (a) Reule, H.; Steeb, S.; Donolato, C. Structure of the Compounds Ag₄Sc, Ag₂Sc, Au₄Sc, Au₂Sc, and Ag₃Yb. *J. Less Common Met.* **1971**, *24*, 108–112; (b) Schuster, J. C.; Bauer, J. The Ternary Systems Sc–Al–N and Y–Al–N. *J. Less Common Met.* **1985**, *109*, 345–350; (c) Zachwieja, U. Synthesis and Structure of CaAu₂ and SrAu₂. *J. Alloys Compd.* **1996**, *235*, 12–14; (d) Nowotny, H.; Mohnheim, A. Die Kristallstruktur von Al₂Ca. *Z. Kristallogr., Kristallgeo., Kristallphys., Kristallchem.* **1939**, *100*, 540–542; (e) Pietrokowsky, P. The Partial Constitutional Diagram TiAu₂–Au: Lattice Parameters of the Alpha Solid Solutions and the Intermediate Phase TiAu₄. *Inst. Met.* **1962**, *90*, 434–438; (f) Schuster, J. C.; Ipsen, H. Phases and Phase Relations in the Partial System TiAl₃–TiAl. *Z. Metallkunde* **1990**, *81*, 389–396.
22. (a) Fornasini, M. L.; Iandelli, A.; Pani, M. Different Stacking of the Gold and Silicon Atoms in the Phases RAuSi (R = Sc, Y, Lu). *J. Alloys Compd.* **1992**, *187*, 243–247; (b) Bockelmann, W.; Schuster, H.-U. *Z. Anorg. Allg. Chem.* **1974**, *410*; (c) Bockelmann, W.; Jacobs, H.; Schuster, H.-U. *Z. Naturforsch. B* **1970**, *25*; (d) Wenski, G.; Mewis, A. REPTX Compounds with Structures Related to AlB₂- and MgAgAs-Type (RE = Y, Rare Earth Element; X = P, As, Sb). *Z. Kristallogr.* **1986**, *176*, 125–134; (e) Pöttgen, R.; Borrmann, H.; Felser, C.; Jepsen, O.; Henn, R.; Kremer, R. K.; Simon, A. Crystal and Electronic Structures of ScAuGe, CeAuGe, and LuAuGe: A Transition from Two- to Three-Dimensional [AuGe] Polyanions. *J. Alloys Compd.* **1996**, *235*, 170–175; (f) Hoffmann, R. D.; Pöttgen, R. AlB₂-Related Intermetallic Compounds – A Comprehensive View Based on Group-Subgroup Relations. *Z. Kristallogr. Cryst. Mater.* **2001**, *216*, 127–145.
23. Dronskowski, R.; Bloechl, P. E. Crystal Orbital Hamilton Populations (COHP): Energy-Resolved Visualization of Chemical Bonding in Solids Based on Density-Functional Calculations. *J. Phys. Chem.* **1993**, *97*, 8617–8624.
24. Jepsen, O. B., A.; Andersen, O.K., The Program TB-LMTO-ASA, version 4.7; Max-Planck-Institut für Festkörperforschung, Stuttgart, Germany, **1999**.
25. Lambrecht, W. R. L.; Andersen, O. K., Minimal Basis Sets in the Linear Muffin-Tin Orbital Method: Application to the Diamond-Structure Crystals C, Si, and Ge. *Phys. Rev. B* **1986**, *34*, 2439–2449.
26. Pušelj, M.; Schubert, K. Kristallstrukturen der Phasen Au₂Al(h), Au₂Al₁-(r) und Au₂Al₁+(r). *J. Less Common Met.* **1974**, *35*, 259–266.
27. West, C. D.; Peterson, A. W. The Crystal Structure of AuAl₂. *Z. Kristallogr., Kristallgeo., Kristallphys.*, **1934**, *88*, 93–94.
28. Eymond, S.; Parthé, E. Sc₂Al with Ni₂In structure Type. *J. Less Common Met.* **1969**, *19*, 441–443.
29. Palenzona, A.; Manfrinetti, P. The Phase Diagram of the Sc–Au System. *J. Alloys Compd.* **1997**, *257*, 224–226.
30. (a) Frank, K.; Schubert, K. Kristallstruktur von AuAl. *J. Less Common Met.* **1970**, *22*, 349–354; (b) Aldred, A. T. Intermediate Phases Involving Scandium. *Trans. Metallurgical Soc. AIME* **1962**, *224*, 1082–1083; (c) Dwight, A. E.; Kimball, C. W., ScT₂X and LnT₂X Compounds with the MnCu₂Al-Type Structure. *J. Less Common Met.* **1987**, *127*, 179–182.
31. Schob, O.; Parthe, E. AB Compounds with Sc, Y and Rare Earth Metals. I. Scandium and Yttrium Compounds with CrB and CsCl Structure. *Acta Crystallogr.* **1965**, *19*, 214–224.
32. Hamilton, W. Significance Tests on the Crystallographic R Factor. *Acta Crystallogr.* **1965**, *18*, 502–510.
33. Hulliger, F. On New Rare Earth Gold Aluminides LnAuAl. *J. Alloys Compd.* **1993**, *200*, 75–78.

For Table of Contents Only



The origin of the hexagonal ScAuAl structure, in which the unit-cell is distorted due to alternating long-short Au–Au chains along the c -axis, is rationalized using electronic structure theory. Models examining Sc, Au, and Al site distributions indicate a structural preference to maximize shortest Au–Al contacts followed by Sc–Au. Chemical pressure effects from atomic size variation and valence electron counts along the polar intermetallic compound series CaAuAl–ScAuAl–TiAuAl were also examined.
